Integrated Sensing and Actuation of Dielectric Elastomer Actuator

Zhihang Ye and Zheng Chen

Department of Electrical Engineering and Computer Science
Wichita State University, 1845 Fairmount St.
Wichita, KS 67260-0083

ABSTRACT

Dielectric elastomer (DE) is a type of soft actuating material, the shape of which can be changed under electrical voltage stimuli. DE materials have great potential in applications involving energy harvesters, micromanipulators, and adaptive optics. In this paper, a stripe DE actuator with integrated sensing and actuation is designed and fabricated, and characterized through several experiments. Considering the actuator's capacitor-like structure and its deform mechanism, detecting the actuator's displacement through the actuator's circuit feature is a potential approach. A self-sensing scheme that adds a high frequency probing signal into actuation signal is developed. A fast Fourier transform (FFT) algorithm is used to extract the magnitude change of the probing signal, and a non-linear fitting method and artificial neural network (ANN) approach are utilized to reflect the relationship between the probing signal and the actuator's displacement. Experimental results showed this structure has capability of performing self-sensing and actuation, simultaneously. With an enhanced ANN, the self-sensing scheme can achieve 2.5% accuracy.

1. INTRODUCTION

Many soldiers and civilians lose their hands, arms and legs on battlefields, in accidents, and as the result of natural disasters. Also, many senior people partially or completely lose the functioning of a limb due to the aging process. To help these handicapped people, many researchers have spent years of effort on developing prosthetic or exoskeleton devices to restore limb's functions. Although recent technologies and theories are far from fully simulating the functions of legs and arms,[1,2] the prosthetic research is capturing the attention of researchers. Most research is based on electrical motor-driven prosthetic limbs, varying from a single finger to a full arm.[3,4] Companies such as DEKA have developed commercial robotic arms controlled by electric motors.[5] For a more compact structure and higher efficiency, many researchers, inspired by biological muscles, used a tendon-driven structure in their designs.[6] Although of this work shows great potential for a bio-inspired design of prosthetic arm or leg, a compliant actuator is still missing.

To overcome the limits of an electrical motor, many researchers turn to investigate the feasibility of using smart materials in prosthetic limb designs. A well-known smart material is called electroactive polymer (EAP), which has unique properties, such as flexibility, light-weight, bio-compatibility, and high energy-efficiency.[7] Dielectric elastomers (DE) are an important kind of electronic EAPs. A typical DE actuator consists of two main structures: a thin layer of elastomer material and compliant electrodes.[8] When voltage (higher than 1000 V) is applied to the electrodes, the electrostatic force between both electrodes will make the elastomer contracts along the direction of the electrical field between its electrodes.[8] Pelrine studied DE actuators and electro-magnetics in terms of energy density (energy per unit mass).[7] It was found that DE artificial muscles have an ideal energy density that is very close to that of human muscles and about eight times greater than that of electro-magnetics.[7] Many studies have also shown that with DE artificial muscles, artificial limbs are capable of generating enough force for their daily needs.[9,10] It also shows that an EAP-powered robotic arm has much better future applications than the electric motor-powered arms.

Further author information: (Send correspondence to Zheng Chen)
Zheng Chen: E-mail: zheng.chen@wichita.edu, Telephone: 1-316-978-7391

Electroactive Polymer Actuators and Devices (EAPAD) 2017, edited by Yoseph Bar-Cohen, Proc. of SPIE
Vol. 10163, 101630C · © 2017 SPIE · CCC code: 0277-786X/17/$18 · doi: 10.1117/12.2262358

Downloaded From: https://www.spiedigitallibrary.org/conference-proceedings-of-spie on 4/16/2018 Terms of Use: https://www.spiedigitallibrary.org/terms-of-use

Existing research work in DE material has been mainly focused on improving the DE's actuation capability, modeling, and control of the actuator in applications.[8,10–13] Self-sensing mechanisms of DE actuators have been investigated by a number of researchers.[14–17] Most of the reported approaches were focused on either resistance or capacitive sensing of the DE actuator, based on the fact that the capacitance and resistance depend on the strain of the actuator. Self-sensing was integrated in the output feedback control of the DE actuator.[18] However, due to the noise of the capacitive reading and the drift of the capacitance-strain rate, it is challenging to achieve satisfactory control performance.[18]

In this paper, a DE artificial muscle with integrated sensing and actuation is developed. This strip actuator presents muscle-like shape and actuating style, which makes it capable of bio-inspired actuation in prosthetic applications. Its electrical impedance changes with its strain output, which enables it self-sensing capability. This self-sensing function is performed by adding a high frequency probing signal to a low frequency actuation signal and then using FFT method to extract electrical impedance in high frequency from the actuator's current and voltage measurement. Further study revealed that the actuation dynamic of the actuator is a low-pass filter and the high frequency signal has minor impact on its actuation performance, which enables the actuator for simultaneous actuation and sensing. By adjusting the probing signal's frequency to a proper value, the probing signal can be well separated from the base driving input and channel noise from the data acquisition equipment, which also gives better sensing results, and the required sensing power is limited within an acceptable range. The effect of probing frequency on self-sensing has been investigated and an optimal probing frequency has been found out based on the experimental data. More over, an artificial neural network (ANN) is introduced to estimate the displacement output based on the processed FFT data, which shows a better prediction than a polynomial fitting method. Experimental results show that ANN based estimation makes the self-sensing method more robustness to high sensing noise in real-world applications.

The rest of the paper is organized as follows: Design and fabrication of the actuator is shown in Section 2. Experimental results are discussed in Section 3. Section 4 shows how to improve the accuracy of displacement prediction with the ANN network. Conclusions and future work are discussed in Section 5.

2. DESIGN AND FABRICATION OF BIO-INSPIRED ARTIFICIAL MUSCLE

A cross-sectional view of the actuator design is shown in Fig. 1. The actuator has typical sandwiched structure. A DE material is placed in the middle of the structure. Compliant electrodes can be made by pasting carbon particles, metal powders, or other soft, conductive materials on both sides of the DE material. Bonding materials, such as 3M VHB tape or conductive PDMS polymer, are used to bond the connecting wire with the DE actuator in the bonding area. On the other side of bonding material's area, a small supporting plate is attached to the DE material to maintain the actuator's shape when it deforms. Specifically, if a conductive PDMS[19] is used as the bonding material, this could significantly secure the electrical connection between the wires and electrodes on the dielectric elastomer. However, fabrication of the conductive PDMS with low resistance and high compliance is challenging, which will be focused in the future work.

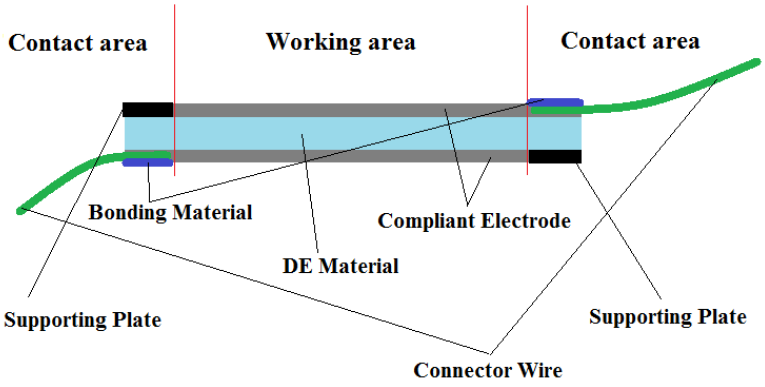

Figure 1. Design of bio-inspired artificial muscle.

Downloaded From: https://www.spiedigitallibrary.org/conference-proceedings-of-spie on 4/16/2018 Terms of Use: https://www.spiedigitallibrary.org/terms-of-use

An actuator sample was also fabricated for later experiments. A 3M VHB 4905 tape strip of 15×7.5 cm size was cut from a tape roll. The strip was stretched in the longitudinal direction by 100%, and fixed in this state. Then, two wood plates, 10×1 cm size, were attached in the middle of the stretched VHB strip and used as supportive components to maintain the shape of the actuator. Before pasting compliant electrodes, the edges of the DE membrane were marked with a pen so that the edges were isolated from each other to avoid electrical sparking. Inside the marked area, graphite powders (Hillman Inc.) were pasted on both surfaces of the VHB membrane as compliant electrodes. After the electrode material were spread generously on the surfaces, the whole device was cut from the base strip. The device was nearly 9.4×10 cm, and the elliptical shape in the middle was due to the one-directional pre-stretching before cutting off the device.

3. EXPERIMENTAL RESULTS

3.1 Actuation Dynamics

As shown in the experimental setup in Fig. 2(a) the actuator was vertically fixed on a metal frame. A calibration weight load (100 gram) was attached on the lower end of the actuator. A driving voltage was generated by a dSPACE real-time control system and a high-voltage amplifier (5HVA24-BP1-F, UltraVolt Inc.). When the driving voltage was applied, the DE material created a compression in thickness, and the internal change of stress interacted with the external stretching force, which made the load move lower than its original position. When the driving voltage was off, the DE material's internal stress was restored to its former level, and the load moved back to its original position. A Baumer OADM 20I6441/S14F displacement laser sensor placed under the weight load was used to capture load movements. A high voltage amplifier (5HVA24-BP1-F, UltraVolt Inc) was used to generate a up to 5,000 V voltage that was applied to the actuator. To drive the device, the actuation voltage was set between 100 and 4,900 V. A high-frequency probing voltage was added to the actuation voltage. Both voltage and current were measured by a dSPACE's real-time control system (). The sampling rate of the dSPACE's ADC units was set to 1 kHz.

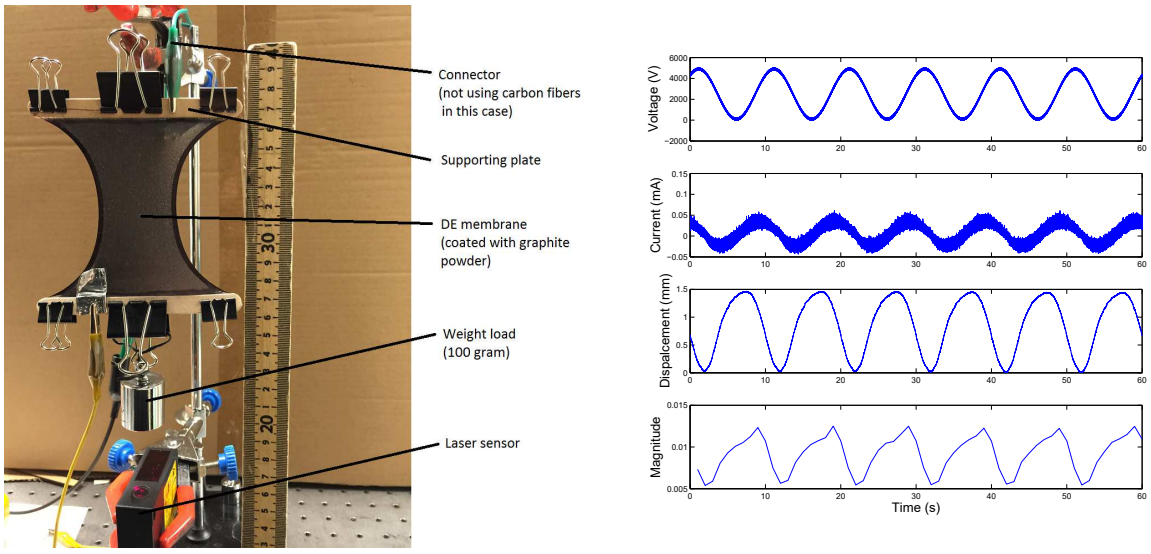

(a) (b)

Figure 2. First test of self-sensing capability: (a) experimental setup; (b) experimental results.

In the first test, the actuation voltage was a sinusoidal wave with 0-4900 V (peak to peak) and 0.1 Hz. The amplitude and frequency of the probing voltage were set at 100 V and 50 Hz, respectively. Fig. 2(b) shows the experimental results, where the first sub-figure shows the voltage applied to the actuator, including actuation voltage and probing voltage. The second sub-figure shows the measured current. The third sub-figure shows the displacement of weight load. The last sub-figure shows the magnitude of the current at the probing frequency. From Fig. 2(b), one can see that there is a non-linear relation between the displacement and the magnitude.

Downloaded From: https://www.spiedigitallibrary.org/conference-proceedings-of-spie on 4/16/2018 Terms of Use: https://www.spiedigitallibrary.org/terms-of-use

When the strip deformed, its length increased which led to a higher surface resistance and caused a decrease in the current magnitude. Hence, it is possible to find the mapping relation from the magnitude to the displacement of the actuator.

Before determining the relationship between the actuator's displacement and the probing signal, an empirical method was used to find a transfer function to approximate the actuation dynamics of the actuator. This procedure was conducted using the same experimental setup, and sinusoidal voltage inputs with different frequencies and magnitudes were fed to the actuator. All the displacement data was recorded, and FFT was performed to obtain the magnitude of the current response. The full voltage input range (0 - 5000 V) was normalized between 0 and 1. A frequency response of the actuator without probing signal was collected and a third-order transfer function with a cut-off frequency of 10.5 rad/s was used to approximate it, which is shown in Fig. 3(a). To investigate the impact of probing signal on the actuation dynamics, a frequency response of the actuator with a probing signal (0.02 magnitude, 50 Hz) was collected and plotted in Fig. 3(b). Comparing Fig. 3(a) and (b), one can conclude that the frequency responses with and without probing signal are very close and the probing signal does not impact the actuation response. The fitting transfer function for the actuator is shown as follow:

$$G(s) = \frac{0.09537s^2 + 1.681s + 11.05}{0.002286s^3 + 0.1159s^2 + 1.509s + 1}. \quad (1)$$

Considering the actuator's cut-off frequency, the probing signal's frequency should be higher than 21 rad/s.

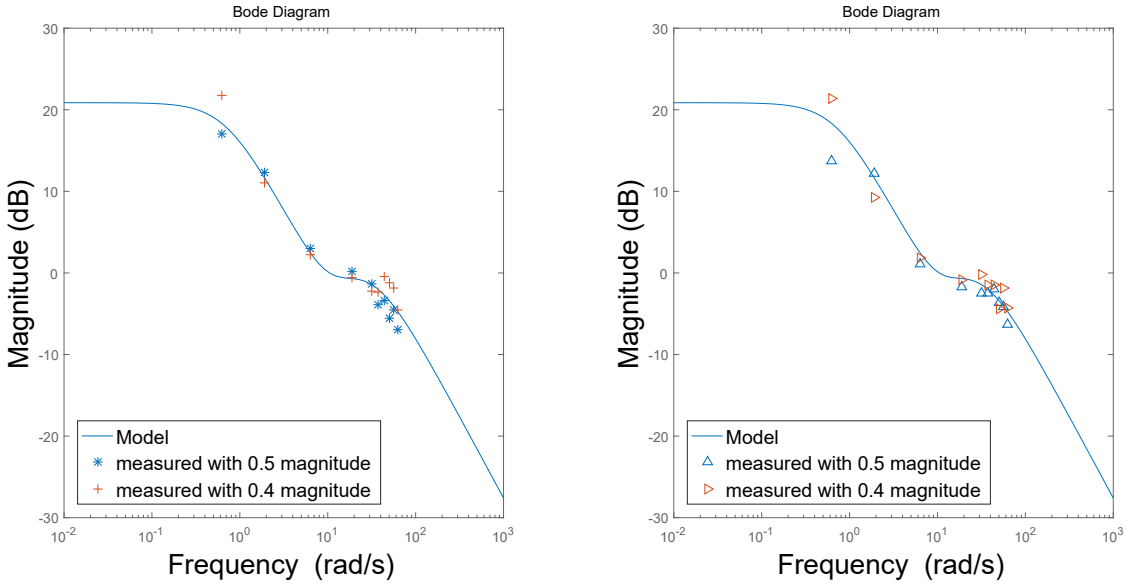

(a) (b)

Figure 3. (a) Model without probing signal; (b) Model with probing signal added.

3.2 Self-Sensing with Polynomial Curve-Fitting Method

Polynomial curve fitting is a useful tool to obtain the mapping relationship. Based on former experimental settings, data over a continuous four minutes was collected. A polynomial curve-fitting function was extracted form this four minutes of data. Another one minute of data was collected with the same experimental setup and used to verify the mapping function that was obtained from former experiments. Fig. 4(a) shows a second-order polynomial curve-fitting result of the four minutes of data. The measured and estimated displacements are plotted in Fig. 4(b).

To investigate the impact of probing frequency on the self-sensing performance, a series of probing signals with the same magnitude but different frequencies (30 - 100 Hz, in 10 Hz steps) were tested in experiments. The

Downloaded From: https://www.spiedigitallibrary.org/conference-proceedings-of-spie on 4/16/2018 Terms of Use: https://www.spiedigitallibrary.org/terms-of-use

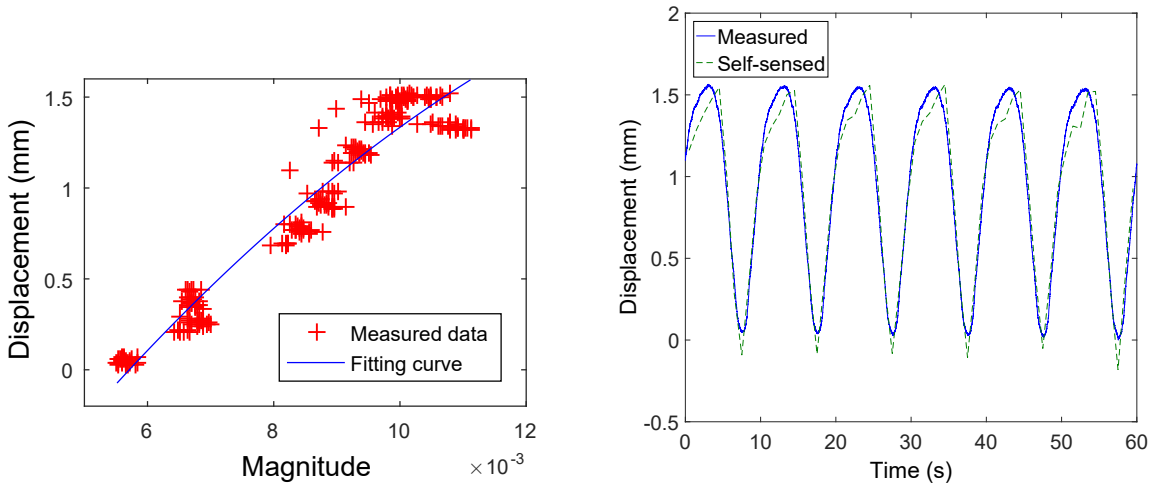

(a) (b)

Figure 4. (a) Second-order polynomial fitting curve of 50 Hz probing signal; (b) Comparison of measured displacement and self-sensed displacement with polynomial fitting.

fitting curves are plotted in Fig. 5. These fitting curves with different probing frequencies have some differences, but the average estimation errors are similar. Table 1 shows the average error with different probing frequencies. Some data sets had an unusually high error level, which was probably due to some issues (disturbance, noise) occurring during the data collection process. But other data sets also had a close error level. Hence, the probing frequency does not have a significant effect on the self-sensing accuracy. In order to minimize power consumption, the probing frequency should be as low as possible. But it is also very important to keep the sensing signal higher than a reasonable value to separate it from the driving signal. From Table 1, one can conclude that 50 Hz was the best probing frequency in terms of both low estimation error and low power consumption.

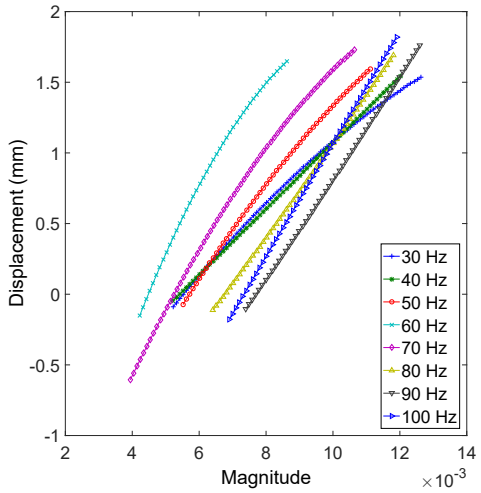

Figure 5. Comparison of fitting curves.

Table 1. Self-sensing error of different probing frequencies.

Probing Frequency (Hz)	30	40	50	60	70	80	90	100
Error (%)	7.77	7.31	6.43	8.44	10.63	7.30	7.65	9.12

Downloaded From: https://www.spiedigitallibrary.org/conference-proceedings-of-spie on 4/16/2018 Terms of Use: https://www.spiedigitallibrary.org/terms-of-use

4. SELF-SENSING WITH ARTIFICIAL NEURAL NETWORK

To reduce the estimation error of the self-sensing, an artificial neural network was employed to estimate the displacement output based on the magnitude of probing current signal. Artificial neural network (ANN) is a powerful tool for non-linear fitting. An ANN consists of one or several layers of artificial neurons. In a typical three-layer ANN, the first layer is referred to as the input layer, a hidden layer connects the input layer, and the last layer is called the output layer. Neurons in the hidden layer are connected to neurons in the first and last layers. Each neuron has its weight, bias, and transfer function, and with the help of training data and a specific training algorithm, all neurons are changing their weight and bias values to achieve the nonlinear fitting goal.[20]

In this study, two types of ANN, normal ANN and enhanced ANN, were employed for estimating the displacement output. Same data sets were used again for training the ANNs to fit the curve between the measured magnitude and the displacement. In the first test, a three-layer back-propagation (BP) neural network, which is a normal ANN, was built and trained by previous four minutes of data. Then the last one minute of data was used to verify the network. Fig. 6(a) shows the fitting curve done by the neural network, and Fig. 6(b) shows the displacement curve, the sensed value of displacement peak were not very ideal, but the overall error level was much better than polynomial curve fitting. With the neural network, the error level was 2.74%, less than half of the former fitting result. Probing signals with different frequencies were also tested with neural network. In addition to some data sets being largely affected by noise or disturbance, all data sets showed a decreasing error level. Fig. 7(a) shows the fitting curves of all frequencies, and the average error level is shown in Table 2.

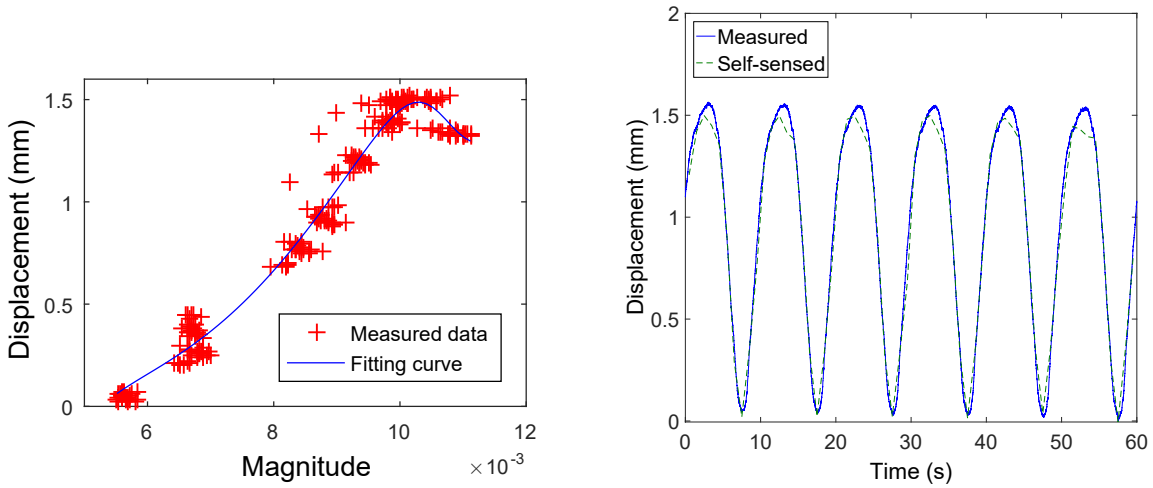

(a) (b)

Figure 6. (a) Neural network fitting curve of 50 Hz probing signal; (b) Comparison of measured displacement and self-sensed displacement with ANN fitting.

In order to obtain more accurate and robust self-sensing results, an enhanced ANN with additional data-handling methods were used in following calculation: First, the FFT window was changed. In the former tests, each FFT window contained 1,000 data points and was separated, which means 60 data could only give 60 data points. For more data points from a data set of the same length, a rolling window was employed during data extraction. The length of the FFT window was still 1,000 points, but each time the window was moved 500 points forward, the number of data point was doubled. Second, the input of the neural network did not have only one value but rather included one current magnitude value and one latest historical magnitude value. In this way, the neural network could discern the trend of the device's displacement. The neural network had four neurons in this case, and worked with at least two magnitude-displacement data points. The fitting results of the 50 Hz probing signal has an average error level of 2.62% (compared to 2.74%); therefor, for well-collected data, these additional data processing methods would not give obvious enhancement of the fitting accuracy. But when it came to heavily compromised data, such as data with a 70 Hz probing signal, the average error was diminished

Downloaded From: https://www.spiedigitallibrary.org/conference-proceedings-of-spie on 4/16/2018 Terms of Use: https://www.spiedigitallibrary.org/terms-of-use

by nearly half of its former level. The error was 11.54% before, and in this case it was only 5.30%. In summary, the overall fitting results with extra processing methods are shown in Fig. 7(b). By comparing these results with the former fitting results, it can be seen that the pattern of each fitting curve is more unified, which means that the fitting result is more robust than previously. In Table 2, the accuracy improvement of compromised data is also apparent.

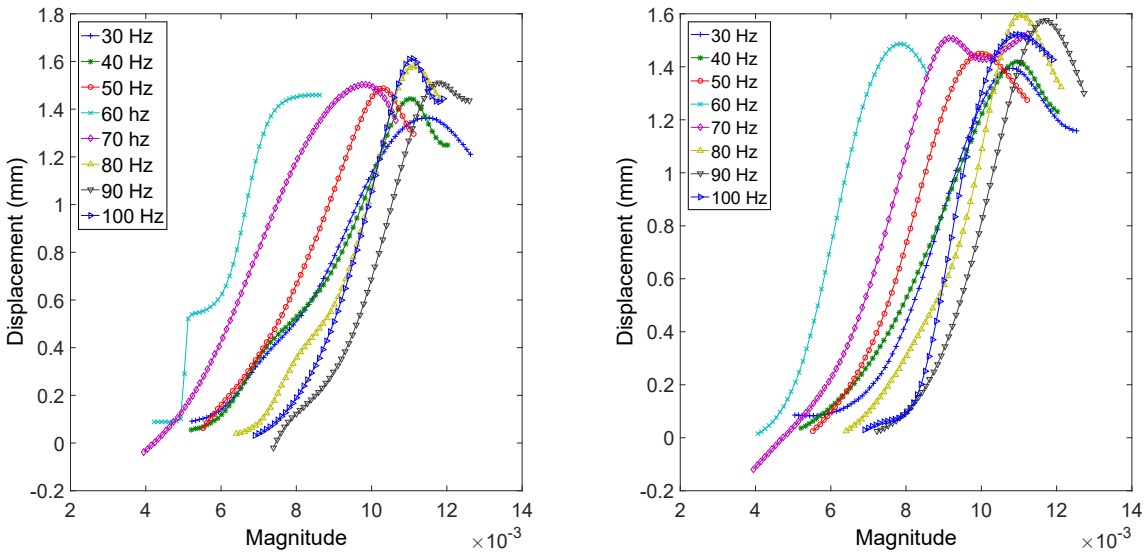

Figure 7. (a) Comparison of ANN fitting curves.; (b) Comparison of enhanced ANN fitting curves.

Table 2. ANN Self-sensing error of different probing frequencies.

Probing Frequency (Hz)	30	40	50	60	70	80	90	100
Error of normal ANN (%)	4.67	3.13	2.74	6.31	11.54	4.56	6.90	4.80
Error of enhanced ANN (%)	4.18	2.32	2.62	3.25	5.30	2.48	2.72	4.75

5. CONCLUSIONS AND FUTURE WORK

In this paper, a strip DE actuator with integrated sensing and actuation capability has been developed. A sample of strip actuator has been designed, fabricated, and characterized. A self-sensing scheme has been developed to capture the displacement output of the actuator based on its high frequency impedance measurement. The study has shown that the probing signal at high frequency does not impact the actuation performance so that the actuator is capable of performing simultaneous sensing and actuation. This great self-sensing feather enables us to measure the actuator's deforming states without adding additional sensors, which makes the actuation system more compact and easy to adapt to prosthetic applications. The self-sensing tests have also shown that the fitting method played an important role in improving the self-sensing accuracy. Three different fitting approaches, second-order polynomial fitting, normal ANN, and enhanced ANN have been used to estimate the self-sensed displacement, of which the enhanced ANN has been found out the best fitting approach.

Future work will be focused on improving the accuracy of self-sensing. Using different materials and the shape of device will have a significant effect on self-sensing as well as actuation. From the experimental results, the advanced data processing method could help considerably in achieving a higher accuracy. How to implement this self-sensing method in feedback control will be focused in the future work.

Downloaded From: https://www.spiedigitallibrary.org/conference-proceedings-of-spie on 4/16/2018 Terms of Use: https://www.spiedigitallibrary.org/terms-of-use

Acknowledgment

This research was supported in part by the National Science Foundation under CAREER Grant DCSD #1653301 and Multidisciplinary Research Project Award (MURPA) Wichita State University.

REFERENCES

1. R. Bogue, "Exoskeletons and robotic prosthetics: a review of recent developments," *Industrial Robot: An International Journal* **36**(5), pp. 421–427, Emerald Group Publishing Limited, 2009.
2. J. Lai, M. Schoen, A. P. Gracia, D. Naidu, and S. Leung, "Prosthetic devices: challenges and implications of robotic implants and biological interfaces," *Proceedings of the Institution of Mechanical Engineers, Part H: Journal of Engineering in Medicine* **221**(2), pp. 173–183, SAGE Publications, 2007.
3. B. Massa, S. Roccella, M. C. Carrozza, and P. Dario, "Design and development of an underactuated prosthetic hand," in *Robotics and Automation, 2002. Proceedings. ICRA'02. IEEE International Conference on*, **4**, pp. 3374–3379, IEEE, 2002.
4. E. J. Rouse, L. M. Mooney, E. C. Martinez-Villalpando, and H. M. Herr, "Clutchable series-elastic actuator: Design of a robotic knee prosthesis for minimum energy consumption," in *Rehabilitation Robotics (ICORR), 2013 IEEE International Conference on*, pp. 1–6, IEEE, 2013.
5. DEKA, "The deka arm." www.dekaresearch.com\deka_arm.shtml.
6. Q. M. Li and Y. W. Li, "Anthropomorphic optimization of a rope-driven prosthetic finger," in *Applied Mechanics and Materials*, **568**, pp. 899–903, Trans Tech Publ, 2014.
7. R. Pelrine, R. Kornbluh, J. Joseph, R. Heydt, Q. Pei, and S. Chiba, "High-field deformation of elastomeric dielectrics for actuators," *Materials Science and Engineering: C* **11**(2), pp. 89–100, 2000.
8. Z. Suo, "Theory of dielectric elastomers," *Acta Mechanica Solida Sinica* **23**(6), pp. 549–578, 2010.
9. R. Pelrine, R. Kornbluh, Q. Pei, and J. Joseph, "High-speed electrically actuated elastomers with strain greater than 100%," *Science* **287**(5454), pp. 836–839, 2000.
10. F. Carpi, D. De Rossi, R. Kornbluh, R. E. Pelrine, and P. Sommer-Larsen, *Dielectric elastomers as electromechanical transducers: Fundamentals, materials, devices, models and applications of an emerging electroactive polymer technology*, Elsevier, 2011.
11. L. Liu, Y. Liu, and J. Leng, "Theory progress and applications of dielectric elastomers," *International Journal of Smart and Nano Materials* **4**(3), pp. 199–209, 2013.
12. P. Brochu and Q. Pei, "Advances in dielectric elastomers for actuators and artificial muscles," *Macromolecular rapid communications* **31**(1), pp. 10–36, 2010.
13. F. Carpi and D. De Rossi, "Contractile folded dielectric elastomer actuators," in *The 14th International Symposium on: Smart Structures and Materials & Nondestructive Evaluation and Health Monitoring*, pp. 65240D–65240D, International Society for Optics and Photonics, 2007.
14. B. O'Brien, J. Thode, I. Anderson, E. Calius, E. Haemmerle, and S. Xie, "Integrated extension sensor based on resistance and voltage measurement for a dielectric elastomer," in *Proc. of the SPIE Conference on Electroactive Polymer Actuators and Devices (EAPAD)*, 2007.
15. K. Jung, K. J. Kim, and H. R. Choi, "A self-sensing dielectric elastomer actuator," *Sensors and Actuators A: Physical* **143**(2), pp. 343–351, 2008.
16. N. H. Chuc, D. V. Thuy, J. Park, D. Kim, J. Koo, Y. Lee, J.-D. Nam, and H. R. Choi, "A dielectric elastomer actuator with self-sensing capability," in *Proc. of the SPIE Conference on Electroactive Polymer Actuators and Devices (EAPAD)*, p. 69270V, 2008.
17. T. A. Gisby, B. M. O'Brien, and I. A. Anderson, "Self sensing feedback for dielectric elastomer actuators," *Applied Physics Letters* **102**(19), p. 193703, 2013.
18. S. Rosset, B. M. OBrien, T. Gisby, D. Xu, H. R. Shea, and I. A. Anderson, "Self-sensing dielectric elastomer actuators in closed-loop operation," *Smart Materials and Structures* **22**(10), p. 104018, 2013.
19. C.-X. Liu and J.-W. Choi, "Strain-dependent resistance of pdms and carbon nanotubes composite microstructures," *IEEE transactions on Nanotechnology* **9**(5), pp. 590–595, 2010.
20. R. Rojas, *Neural networks: a systematic introduction*, Springer Science & Business Media, 2013.

Downloaded From: https://www.spiedigitallibrary.org/conference-proceedings-of-spie on 4/16/2018 Terms of Use: https://www.spiedigitallibrary.org/terms-of-use